The maintenance of cytoplasmic domains and nuclear independence

Nils Gustafsson

6 March 2014

Abstract: Anomalous diffusion in the eukaryotic cell cytoplasm and the maintenance of nuclear independence in polynucleated cell structures such as syncytia and coenocytes challenge the wide consensus of cytoplasmic continuity. Here I derive a model of nucleocytoplasmic protein shuttling in pairs of fused cells. The model implies that nuclear independence in syncytia could be maintained by large nuclear to cytoplasmic concentration gradients. In addition, new models of eukaryotic cell evolution suggest the endoplasmic reticulum (ER) may be responsible for forming cytoplasmic compartments affecting diffusion and maintaining independence in syncytia. Fluorescence recovery after photobleaching experiments on ER structure mutants and models of nucleocytoplasmic shuttling in cell-cell fusion experiments provide an insight into the ER mediated compartmentalisation hypothesis.

Contents

Introduction

Membrane compartmentalisation of functionally specialised aqueous spaces separate from the cytosol are central to eukaryotic life[1] (Figure 1). These membrane bound organelles allow for the coexistence of specialised biochemical environments which are mutually beneficial to the cell. Control of the transmission of information in the form of diffusible signalling molecules and peptides in conjunction with the active transport of larger proteins is vital for coordination of organelles within the cell cycle and in responses to external cell environments. Understanding of this signalling behaviour is limited by our understanding of the diffusion of molecules in the cytoplasm which has been observed to be anomalous. Furthermore compartmentalisation appears to be a determining factor beyond the single cell environment. Distinct independent nuclear control of local cytoplasmic environments is observed in polynucleated cells such as muscle syncytia and ***Drosophila melanogaster*** embryonic coenocytes.

Here I propose a model of nucleocytoplasmic protein shuttling, over long time scales, in pairs of fused cells. The model is used to determine if a diffusion barrier between fused cells is a necessary condition to describe experimental results. Furthermore, it is not known how cytoplasmic domains and nuclear autonomy are maintained. It has been proposed however that the endoplasmic reticulum (ER) may have a role to play[2]. As a second aim of this project I investigate the effect of perturbing the ER on nucleocytoplasmic transport in single cells. This has been done using fluorescence recovery after photobleaching (FRAP) experiments on wild type (WT) ***Saccharomyces cerevisiae*** and mutant ***Saccharomyces cerevisiae*** with altered ER architecture.

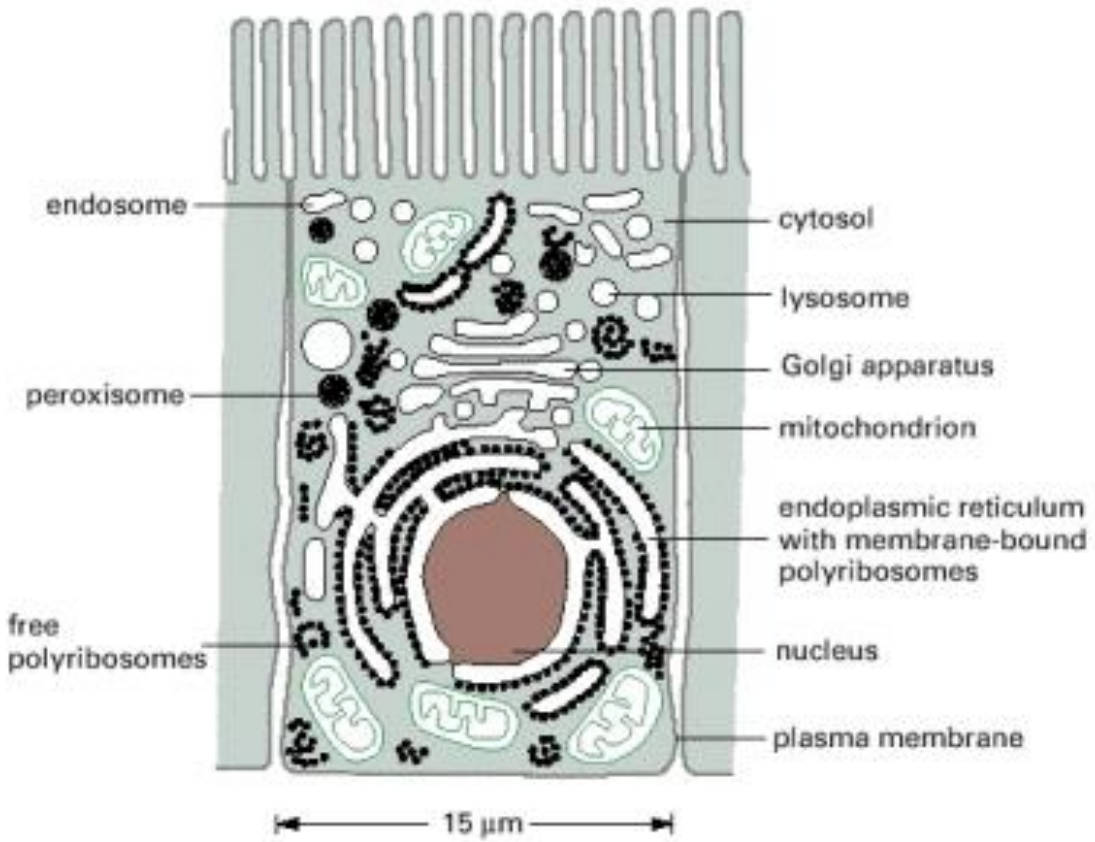

Figure 1: Organelles of the eukaryotic cell. Taken from Molecular Biology of the Cell, Alberts et. al., 2002[1]

Anomalous Diffusion

Anomalous diffusion of small molecules has been widely observed in the cytosol of eukaryotic cells. This anomalous diffusion has been attributed to structural components of the cytoplasm such as F-actin, microtubules and intermediate filaments[3] producing a size dependent sieving with an average pore size in the region of 20-40 nm or other selective filtering effects[4]. There is conflicting evidence however which suggests that observed anomalous diffusion is not molecule size dependent but a result of percolation through pores separating micro compartments of the cytosol[5].

Polynucleated Cell Structures

A large proportion of eukaryotic tissue is found to be polynucleated cell structures either formed by the fusion of multiple single nuclei in the case of syncytia or by multiple nuclear divisions without accompanying cytokinesis in the case of coenocytes. Where it has been looked for the existence of independent nuclear function within the context of these polynucleated cells suggests the ability of nuclei in syncytia and coenocytes to control their local environment. One of the early observations of this made in 1989 showed that organelles including the ER and the Glogi complex as well as structural proteins remained in close proximity to their parent nucleus in cell-cell fusion assays[6]. Other early work identifies domains of transcriptionally distinct nuclei in syncytia close to external inputs such as synapse contacts with myofibers[7,8]. More recently studies of the differentiation of cells in ***Drosophila melanogaster*** embryos[9,10] and the asynchronous mitosis of polynucleated fungal hyphae[11–13] suggest independence of a local cytoplasmic domain, in addition to the ER and Glogi complex, maintained through compartmentalisation or mechanical control by microtubules. The first section of this report outlines a model of the shuttling of proteins, between the nuclei of two fused cells. The presence of a diffusion barrier between fused cells is found to be sufficient but not necessary to explain experimental observations.

The Endoplasmic Reticulum and Cell Architecture

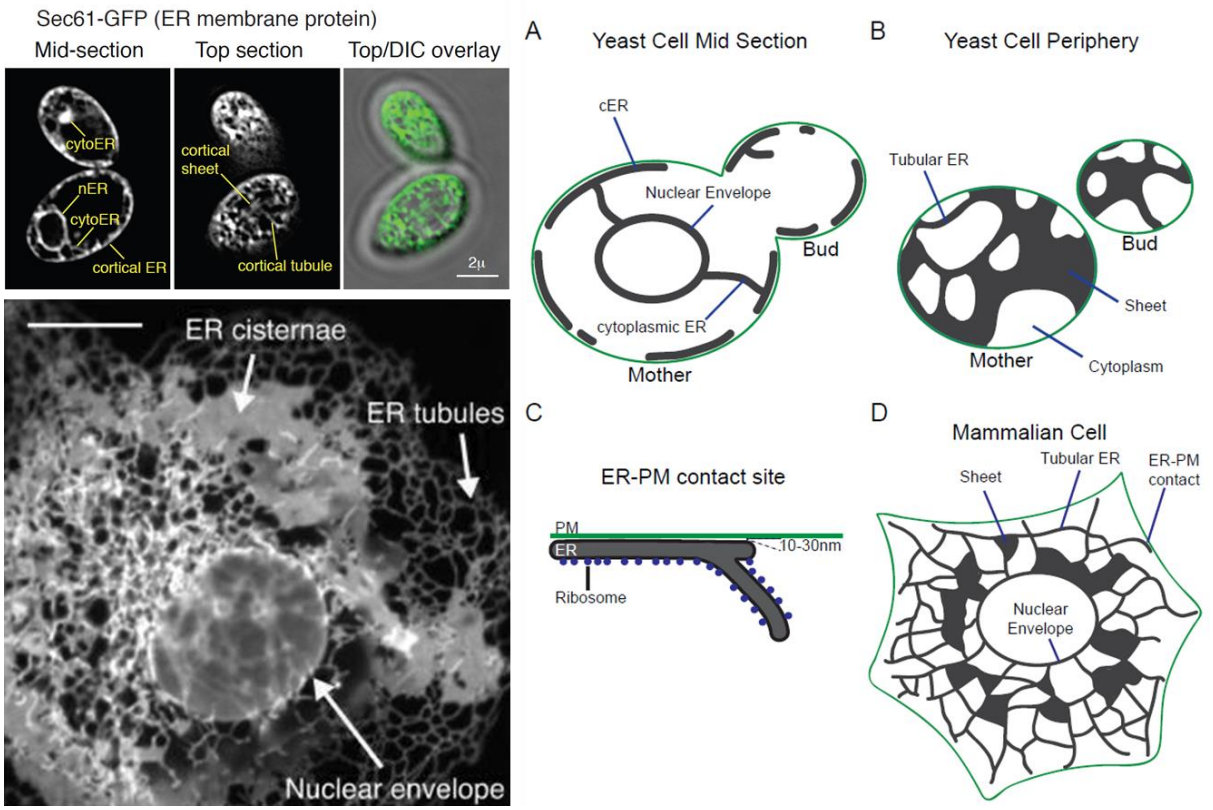

Figure 2: Left panel, Sec61-GFP labelled ER in yeast (top) and mammalian (bottom) cells. Right panel, cartoon representation of the ER structure in yeast cell mid-section (A) periphery (B) PM contact (C) and mammalian Cell (D). Taken from Friedman and Voeltz, 2011[14] and Stefan et. al., 2013[15].

It is not known how cytoplasmic domains and nuclear autonomy are established. It has been proposed that the endoplasmic reticulum (ER) may have a role to play.[2] The ER is a single, large, membrane bound organelle. It has a continuous lumen and is itself continuous with the nuclear envelope (NE). It has an elaborate 3-dimensional structure made up of both flat cisternal regions and cylindrical tubular regions which extend throughout the cell[14] (Figure 2). The ER has a number of roles including in protein synthesis by ER associated ribosomes and in lipid and carbohydrate metabolism. Furthermore the ER maintains contacts via tethering proteins to nearly every membrane bound organelle in the cytoplasm and to the plasma membrane (PM). It has been shown that these contacts facilitate signalling between organelles and between organelles and the PM[15]. Loss of ER tethering proteins results in a dramatic change in ER structure[16]. Visual inspection (Figure 2) of the structure of the ER supports the hypothesis[2] that the ER may compartmentalise the cytoplasm, and thus cause anomalous diffusion, particularly in mammalian cells where the ER network is significantly more extensive. The second part of this report describes FRAP experiments which I carried out on WT yeast cells and mutant yeast cells lacking the ER tethering proteins. The rate of recovery of nuclear GFP fluorescence was measured to infer nucleocytoplasmic transfer rates. These initial tests were designed to set up an experimental system to establish the extent of cytoplasmic domain formation by the ER.

Modelling Nucleocytoplasmic Protein Shuttling In Fused Cells

Background of Fused Cell Experiments

Single or multiple cell-cell fusion events can be triggered in culture, to study behaviour in syncytia, by transfecting cells with bacterial fusion proteins. These assays can be combined with expression of fluorescently tagged nuclear localising signals (NLSs) and nuclear export signals (NESs). These are

modular polypeptide sequences responsible for active nuclear import and export respectively through nuclear pore complexes (NPCs). This system has been used previously in conjunction with FRAP as a live-cell nucleocytoplasmic shuttle assay[17] but no studies of the evolution of the system in time from fusion to equilibrium have been published.

B. Baum has performed this fusion assay between HeLa cells transfected with GFP-NLS bacterial plasmid and HeLa not transfected with any fluorescent proteins. The GFP-NLS expressing cells are identified in fluorescence microscopy as having very high average intensities in the nucleus as compared to the un-transfected cells which are dark. Cell-cell fusions between these two cell types are observed in phase contrast and a change in the fluorescence intensities of the previously fluorescent nucleus (donor) and the previously dark nucleus (acceptor) can be observed as GFP-NLS is accumulated in the acceptor nucleus.

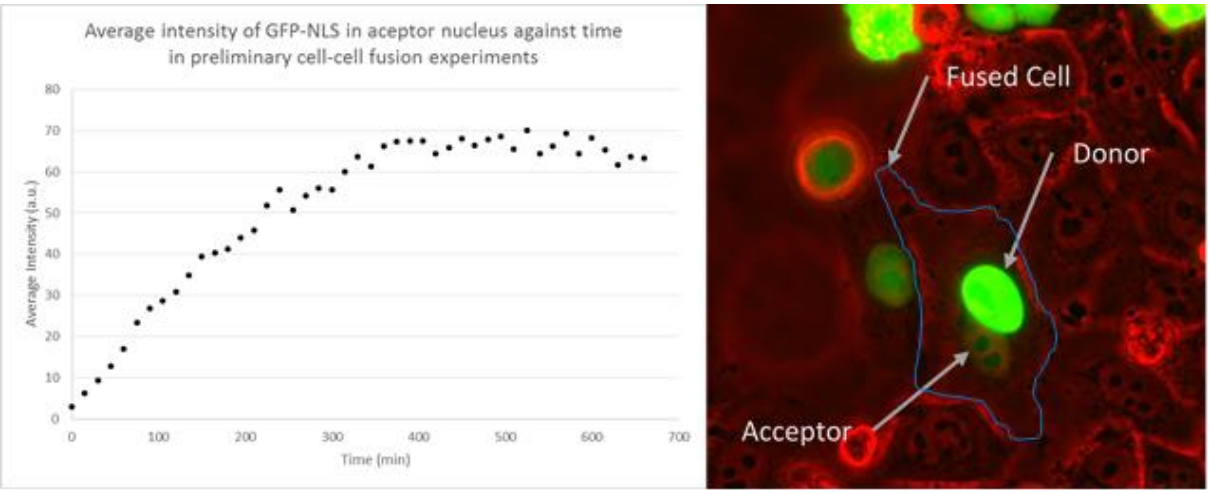

Figure 3: Preliminary cell-cell fusion experiments. Left panel, average intensity of the Acceptor nucleus against time after fusion. Right panel, cell-cell fusion data at 150 minutes after fusion event, GFP-NLS fluorescence signal in green, phase contrast in red.

The average intensity of GFP in a region of interest (ROI) is proportional to its concentration, [GFP], which means average intensity (a.u.) in the acceptor nucleus can be used as a proxy for [GFP-NLS] in the acceptor nucleus[18]. Preliminary data from these experiments[†] show that steady state equilibrium of [GFP-NLS] is not reached for 300-400 minutes (Figure 3). From the beginning of the experiment and beyond this time point the GFP signal in the donor nucleus is saturated indicating a much higher [GFP-NLS] in the donor even after steady state is reached. These observations suggest nuclear independence is maintained after fusion despite close spatial proximity of the two nuclei.

Single Cell Model Formulation

A single cell model (Figure 4) of cytoplasmic and nucleoplasmic concentrations of an mRNA and its associated protein, P, was developed as a basis for modelling the donor-acceptor fluorescence in the cell-cell fusion experiments. This model was also used to fit the FRAP data for the single yeast cell experiments.

The two mechanisms, passive diffusion and active transport, which account for nuclear-cytoplasmic exchange across the NE can be considered independent[19] and as such are decoupled in the model. It is also assumed that the cytoplasm and nucleoplasm are well mixed systems with fast diffusion of small molecules relative to active or passive transport across the NE[20]. The surface integrated passive

[†] Data from experiments performed by B. Baum

flux across the NE $\boldsymbol{J}_{pass}$ (mol/s) has been found empirically to be proportional to the concentration gradient between the nucleus and the cytoplasm[21] and so can be defined as

$$\boldsymbol{J}_{pass} = D_1\left([P]_{cp} - [P]_{np}\right) \quad 1$$

where $[P]_{cp}$ is the cytoplasmic concentration of the protein, $[P]_{np}$ is the nucleoplasmic concentration of the protein and D_1 is the constant of proportionality which encapsulates the system specific characteristics including pore dimensions and molecule size. The surface integrated flux across the NE due to active transport is given by $\boldsymbol{J}_{act}^{c\to n}$ into the nucleus and $\boldsymbol{J}_{act}^{n\to c}$ out of the nucleus. Defined as,

$$\boldsymbol{J}_{act}^{c\to n} = D_2[P]_{cp} \quad 2$$

$$\boldsymbol{J}_{act}^{n\to c} = -D_3[P]_{np} \quad 3$$

where D_2 and D_3 are the rate constants encapsulating the kinetics of import and export respectively. Flux across the NE is defined as positive when the direction is from cytoplasm to nucleoplasm.

The time scale for the cell-cell fusion experiments is of the order of 100s of minutes which is similar to the time scales of protein expression and folding so protein synthesis and degradation must be included in the model. Neglecting to consider plasmid degradation and cell growth the cytoplasmic concentration of mRNA is given by a constant rate of production, R_1, and a first order decay rate k_1.[22,23]

$$\frac{d[mRNA]_{cp}}{dt} = R_1 - k_1[mRNA]_{cp} \quad 4$$

The synthesis of P is assumed to follow first order kinetics with rate k_2 and to follow a first order decay with rate k_3.[24] The cytoplasmic concentration of P is then given by these kinetics less the flux into the nucleoplasm (equation 5).

$$\frac{d[P]_{cp}}{dt} = -\boldsymbol{J}_{pass} - \boldsymbol{J}_{act}^{c\to n} - \boldsymbol{J}_{act}^{n\to c} + k_2[mRNA]_{cp} - k_3[P]_{cp} \quad 5$$

The concentration of P in the nucleoplasm is then given by the flux into the nucleoplasm less a first order degradation by nucleoplasmic proteasomes with rate k_4 (equation 6).

$$\frac{d[P]_{np}}{dt} = \boldsymbol{J}_{pass} + \boldsymbol{J}_{act}^{c\to n} + \boldsymbol{J}_{act}^{n\to c} - k_4[P]_{np} \quad 6$$

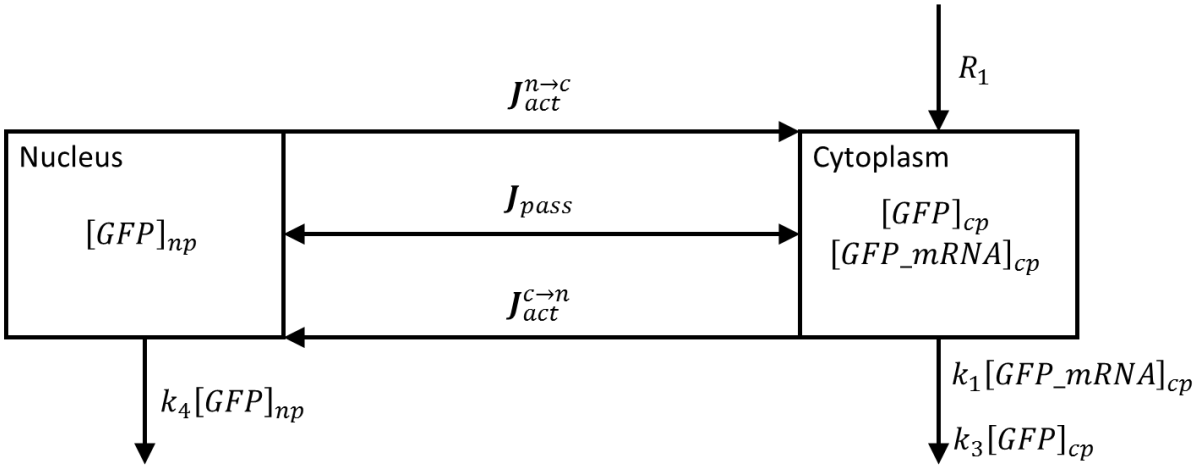

Figure 4: Single Cell Model with two compartments, cytoplasm and nucleoplasm. See text for details

Fused Cell Model Formulation

The single cell model was extended to contain two further compartments, the cytoplasm and nucleoplasm of a second cell. The system is designed such that the only route from the nucleoplasm of the first cell to the nucleoplasm of the second cell is through the cytoplasm of both cells, cp1 and cp2. These two cytoplasm are separated by an artificially imposed diffusion barrier which allows passive diffusion of mRNA and proteins. The surface integrated flux across this diffusion barrier of protein, $\boldsymbol{J}_{pass-P}^{cp1cp2}$, and of mRNA, $\boldsymbol{J}_{pass-mRNA}^{cp1cp2}$, is modelled as proportional to the concentration gradient

$$\boldsymbol{J}_{pass-P}^{cp1cp2} = D_4\left([P]_{cp2} - [P]_{cp1}\right) \quad 7$$

$$\boldsymbol{J}_{pass-mRNA}^{cp1cp2} = D_5\left([mRNA]_{cp2} - [mRNA]_{cp1}\right) \quad 8$$

where D_4 and D_5 become the tuneable parameters of the model to investigate the degree of nuclear independence and cytoplasmic compartmentalisation.

It is assumed that only the first of these cells has been transfected with the means to produce mRNA such that the cytoplasmic concentrations of mRNA are given by

$$\frac{d[mRNA]_{cp1}}{dt} = R_1 - k_1[mRNA]_{cp1} + \boldsymbol{J}_{pass-mRNA}^{cp1cp2} \quad 9$$

and,

$$\frac{d[mRNA]_{cp2}}{dt} = -k_1[mRNA]_{cp2} - \boldsymbol{J}_{pass-mRNA}^{cp1cp2} \quad 10$$

Both cells are assumed to have the ability to translate the mRNA present in their respective cytoplasm such that the cytoplasmic concentrations of protein are given by

$$\frac{d[P]_{cp1}}{dt} = -\boldsymbol{J}_{pass}^{c1\to n1} - \boldsymbol{J}_{act}^{c1\to n1} - \boldsymbol{J}_{act}^{n1\to c1} + \boldsymbol{J}_{pass-P}^{cp1cp2} + k_2[mRNA]_{cp1} - k_3[P]_{cp1} \quad 11$$

and,

$$\frac{d[P]_{cp2}}{dt} = -\boldsymbol{J}_{pass}^{c2\to n2} - \boldsymbol{J}_{act}^{c2\to n2} - \boldsymbol{J}_{act}^{n2\to c2} - \boldsymbol{J}_{pass-P}^{cp1cp2} + k_2[mRNA]_{cp2} - k_3[P]_{cp2} \quad 12$$

The surface integrated fluxes across the respective NE for cell $\boldsymbol{i} = 1$ and cell $\boldsymbol{i} = 2$ are given by

$$\boldsymbol{J}_{pass}^{ci\to ni} = D_1\left([P]_{cpi} - [P]_{npi}\right) \quad 13$$

$$\boldsymbol{J}_{act}^{ci\to ni} = D_2[P]_{cpi} \quad 14$$

$$\boldsymbol{J}_{act}^{ni\to ci} = -D_3[P]_{npi} \quad 15$$

as previously described. This gives a concentration of protein in the nucleoplasm of cell $\boldsymbol{i} = 1$ and cell $\boldsymbol{i} = 2$ of,

$$\frac{d[P]_{npi}}{dt} = \boldsymbol{J}_{pass}^{ci\to ni} + \boldsymbol{J}_{act}^{ci\to ni} + \boldsymbol{J}_{act}^{ni\to ci} - k_4[P]_{npi} \quad 16$$

Bleaching during acquisition changes the proportion of fluorescent protein (FP) which is detected but not the actual amount. This can be corrected for in the data using a bleaching control and appropriate normalisation. Alternatively it can be modelled by first order kinetics. This is calculated as a post processing step. For each time point t for which a measurement is taken, a proportion of the FP is bleached. This proportion is controlled by the parameter k_5 the fraction of FP bleached per image.

The concentration of FP, $[FP]_j(t)$, in compartment j at time t, can then be calculated from the concentration of FP at the previous time an image was taken and the change in the total amount of protein between images,

$$[FP]_j(t) = [FP]_j(t-1) + d[P]_j - k_5\left([FP]_j(t-1) + d[P]_j\right) \quad 17$$

where,

$$d[P]_j = [P]_j(t) - [P]_j(t-1) \quad 18$$

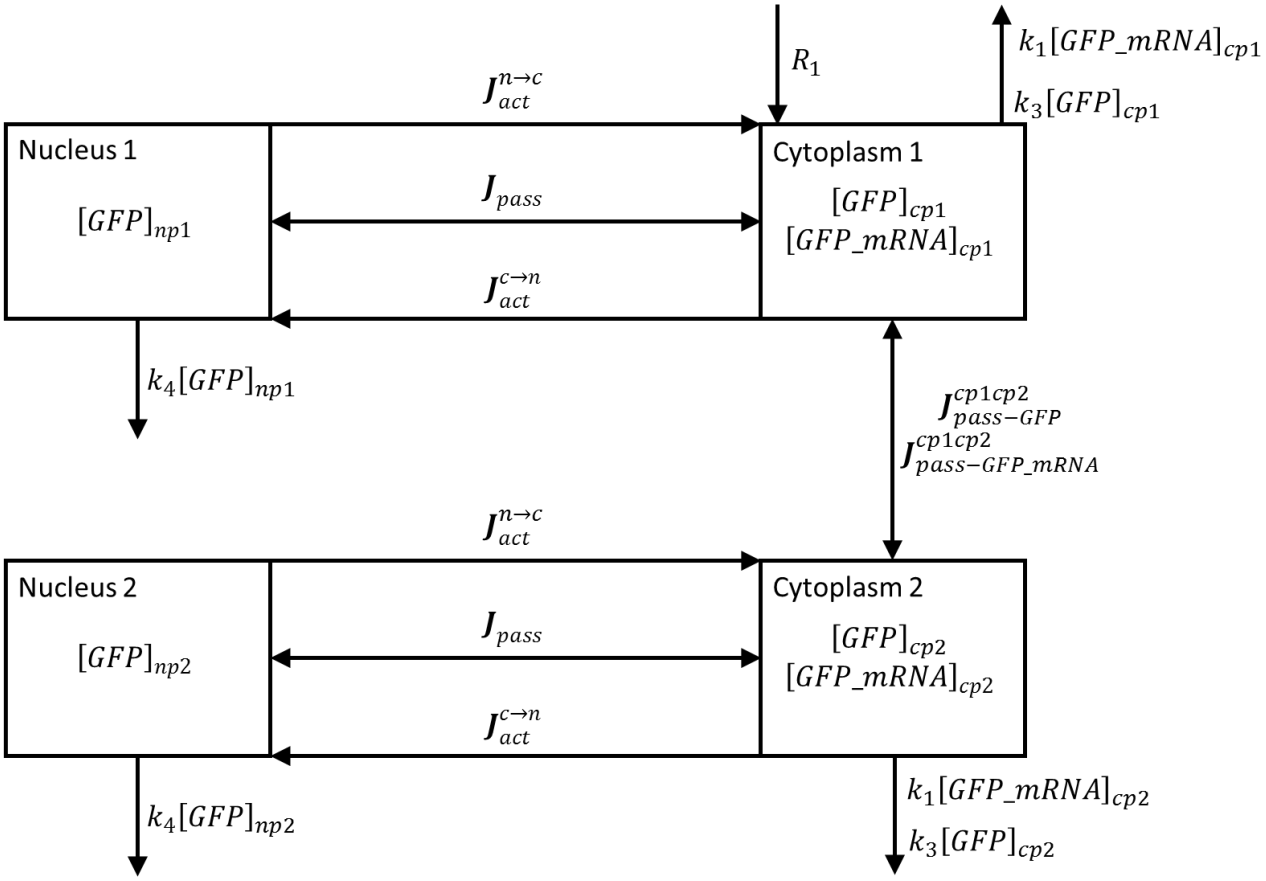

Figure 5: Fused Cell Model, see text for details.

Results and Discussion

The model was integrated numerically using the constant time step Runge-Kutta method[25] implemented using the ordinary differential equation solver in a commercial software package (MATLAB R2013a, The MathWorks Inc., USA). The equations for the single cell model were integrated until steady state concentrations were reached using the initial conditions at transfection, all concentrations equal to 0. The equations for the fused cell model were then integrated until steady state using the steady state concentrations of the single cell models as initial conditions in the donor cell, and 0 for all concentrations in the acceptor cell.

Parameterisation of the model will be expression system and cell dependent. In the absence of necessary controls to determine the parameters they have been estimated where possible from literature or defined by the experimental set up. For example, in the cell-cell fusion experiments for

which there is preliminary data GFP-NLS was used and so no specific active export from the nucleus is possible. This sets the value of $D_3 = 0$.

Order of magnitude approximations of the remaining parameters were determined as follows. The rate of GFP mRNA production has previously been reported between 0.01 molecules cell^{-1} s^{-1} and 1 molecule cell^{-1} s^{-1}, The rate of GFP mRNA degradation has previously been reported between 1x10^{-5} and 1x10^{-3} and the rate of translation has previously been reported as approximately 0.2 s^{-1}.[22,24] To determine the rate of cytoplasmic protein degradation these first three parameters were set to $R_1 = 0.1$ molecules cell^{-1} s^{-1}, $k_1 = 5x10^{-4}$ s^{-1} and $k_1 = 0.2$ s^{-1}, all other parameters were set to zero. The rate of degradation was then tuned such that the half time of GFP production was approximately 90mins, as previously reported,[26] giving $k_3 = 3x10^{-4}$ s^{-1}. The time constant for passive nuclear diffusion of GFP across the NE has previously been reported as approximately 60 seconds.[20] Concentration in the nucleoplasm was set to zero and the passive NE diffusion parameter tuned to produce this time constant giving $D_1 = 1x10^{-3}$ s^{-1}. The preliminary data shows no detectable GFP signal in the cytoplasm of cells transfected with GFP-NLS and a saturated signal in the nucleus. This indicates a large active import rate relative to the passive NE diffusion. D_2 was estimated to be three orders of magnitude greater than D_1 to achieve this. Finally, D_4 and D_5 were set equal to each other and used as a single tuning parameter to fit to the preliminary data. Figure 6 shows the fit to the data in Figure 3 after correcting for bleaching using an unfused cell as a bleaching control and normalising to the arbitrary units of fluorescence. The parameter set used to make this fit is outlined in Table 1 including the rates of diffusion across the artificially imposed diffusion barrier which are $D_4 = 0.1$ and $D_5 = 0.1$. These parameters are two orders of magnitude greater than the NE passive diffusion parameter and allow equilibration of the cytoplasmic concentrations of mRNA and protein to occur on a time scale of seconds. This suggests a very weak diffusion barrier between the two cytoplasm compartments with the time taken to diffuse across approximately equivalent to the time taken to freely diffuse across the cytoplasm of a cell.

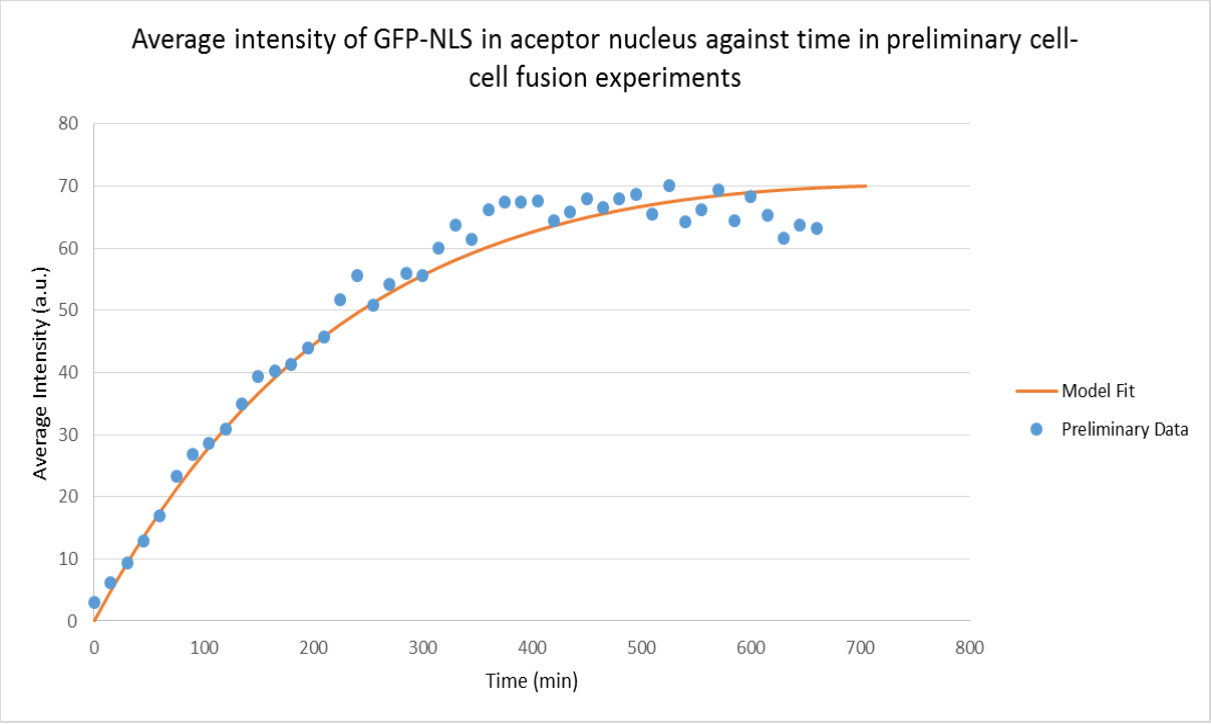

Figure 6: preliminary data from Figure 3. Fit with Fused Cell Model using parameters in Table 1.

Table 1 Parameters for model fit to preliminary data in Figure 6. See text for details

Parameter	Symbol	Dimension	Value
mRNA production	R_1	$(a.u.)\ s^{-1}$	0.1
mRNA degradation	k_1	s^{-1}	5x10^{-4}
Translation	k_2	s^{-1}	0.2
Cytoplasmic protein degradation	k_3	s^{-1}	3x10^{-4}
Nucleoplasmic protein degradation	k_4	s^{-1}	5x10^{-5}
Passive NE diffusion	D_1	s^{-1}	1x10^{-3}
Active NE import	D_2	s^{-1}	1
Active NE export	D_3	s^{-1}	0
Passive protein barrier diffusion	D_4	s^{-1}	0.1
Passive mRNA barrier diffusion	D_5	s^{-1}	0.1

This parameter set which fits the preliminary data is not a unique set and has heavily relied on assumptions of different rate constants. Higher degradation rates in the nucleus for example or lower active NE import rates required a much stronger diffusion barrier between the cytoplasm to fit observations. A simple, one at a time, parameter sensitivity analysis (data not shown) was performed using this parameter set with the univariate output of the model being the half time of GFP concentration in the acceptor nucleus. The most significant parameter was found to be k_4, the nucleoplasmic degradation rate. D_1, D_2 and D_3 were found to have similar significance producing almost as much of a change in the output as k_4. D_4 and D_5 also have an impact on the output but less significantly than those parameters already mentioned. In the range tested the remaining parameters have little or no effect on the GFP concentration half time in the acceptor.

The Role of the Endoplasmic Reticulum Determined by FRAP

FRAP

Fluorescence recovery after photobleaching (FRAP) is an experimental method widely used to study mobility of fluorescent molecules[27]. Commonly used to measure translational diffusion FRAP also enables the quantification of transient binding[28] or transport rates between cell compartments such as organelles or the nucleus[20]. The 1970s saw the first applications of the FRAP method, with Gaussian beam profile bleaching used to study mobility in lipid membranes[29,30]. With the development of the relevant mathematical framework [31,32] and the advent of non-invasive, fluorescent labelling of proteins in live cells, using GFP, resulted in a revival of FRAP in the 1990s[33]. This was aided by the introduction of commercially available confocal microscopes able to perform fast laser power modulation by acousto-optical tunable filters and ROI scanning.

In FRAP experiments a focused, high power light source is used to irreversibly photobleach fluorescent molecules in a small sub cellular ROI. Only the optical properties of the molecules are effected while the dynamics and biochemistry of the molecules remain unchanged[20]. The bleached and fluorescent subpopulations of molecules subsequently begin mixing by diffusion or other active transport mechanisms which results in the recovery of the fluorescent signal in the ROI. The characteristics and rate of the recovery of fluorescence can be used to infer the dynamics of the molecule of interest in the ROI.

Methods

WT and mutant (ΔTether) ***S. cerevisiae*** were transformed with free GFP and mCherry-HDEL. The HDEL fused to the mCherry localises in the ER. The GFP and mCherry-HDEL expression vectors have

been described previously[16] and standard techniques and media were used for yeast transformation and growth.[16]

The nucleus of the cells were identified by the presence of the mCherry labelled, NE associated ER or by inspection of the distribution of GFP fluorescence. At least 10 images were recorded prior to bleaching. A single 100ms exposure, to a circular ROI in the centre of the nucleus, at full laser power was used to bleach the fluorescence in the nucleus. Time-lapse acquisition of the fluorescence recovery starts within 150ms of the end of the bleach pulse with a sampling rate of approximately 3 images per second.

FRAP experiments were performed on mid-log yeast cultures in standard media. Images were acquired on a Leica TCS SP5 inverted confocal microscope (Leica Microsystems AG, Wetzlar, Germany) interfaced with an Ar laser for excitation of EGFP at 488nm and a helium-neon laser for excitation of mCherry at 461nm. A 60x 1.25 numerical aperture oil immersion objective (leica Microsystems) was used, experiments were carried out at 23 °C using laser powers 10-15µW for imaging and fluorescence was recorded on a high speed camera.

Data Analysis

Raw data from the confocal microscope was analysed using FIJI[34] (http://fiji.sc/Fiji). The mean intensity of the ROI in each frame, $I(t)$, was recorded, along with the mean background intensity of each frame, $I_{back}(t)$, and the mean whole cell intensity in each frame, $I_{whole}(t)$. Ten images were taken prior to bleaching and the time averaged mean intensity of the ROI, $\langle I\rangle_{prebleach}$, the background, $\langle I_{back}\rangle_{prebleach}$, and the whole cell, $\langle I_{whole}\rangle_{prebleach}$, were used in normalisation of the data. A three step normalisation was applied to the raw data to correct for fluorescence loss due to photobleaching and allow comparison of different experiments[35].

First normalisation: The first normalisation is a background subtraction and a normalisation of the ROI intensities to their time averaged pre-bleach levels. This first normalisation is used so that experiments with varying prebleach intensities can be compared.

$$I_{norm}(t) = \frac{I(t) - I_{back}(t)}{\langle I\rangle_{prebleach} - \langle I_{back}\rangle_{prebleach}} \qquad 19$$

Second normalisation: The second normalisation is a division by the normalised background subtracted whole cell intensities. This corrects for the fluorescence loss due to bleach pulse and acquisition bleaching. Correction of the fluorescence loss due to the bleach pulse is important to determine the correct mobile/immobile fraction. Correction of the fluorescence loss due to acquisition photobleaching is important as it contributes to the halftime and maximum value of the fluorescence recovery.

$$I_{norm2}(t) = I_{norm}(t)\left(\frac{I_{whole}(t) - I_{back}(t)}{\langle I_{whole}\rangle_{prebleach} - \langle I_{back}\rangle_{prebleach}}\right)^{-1} \qquad 20$$

Third normalisation: The third normalisation is a linear transformation of the range of the data from $[I_{norm}(t_{bleach}), 1]$ to the range $[0,1]$ where $I_{norm}(t_{bleach})$ is the second normalised mean intensity of the ROI in the first frame after bleaching. This normalisation (equation 21) sets the first post bleach intensity to zero for comparison between experiments where a different bleach depth was achieved.

$$I_{norm3}(t) = \frac{I_{norm2}(t) - I_{norm2}(t_{bleach})}{1 - I_{norm2}(t_{bleach})} \qquad 21$$

The data were fitted with a single exponential and compared to the single cell model under FRAP initial conditions.

Results and Discussion

Repeated bleach recovery curves on same nucleus show no differences other than loss of intensity due to photobleaching which implies no photo damage or crosslinking occurs during the bleach pulse or the time-lapse imaging. Full recovery of the fluorescence signal after correcting for fluorescence loss due to photobleaching implies no immobile fraction as expected for unbound GFP. When the bleached ROI is fully contained within the nucleus the recovery half-life shows no dependence on size of the bleach spot which implies that the recovery is not diffusion limited. Limiting factor is nucleocytoplasmic exchange.

Data shown in Figure 7 is the mean of 10 WT recovery curves and 5 ΔTether recovery curves normalised as described in the methods. Error bars show the standard deviation. Fitted curves are found using a simplification of the single cell model. The time scale of FRAP experiments is of the order of 10s of seconds so it is assumed that any biochemistry such as synthesis and degradation of GFP is in steady state. We can assume that total GFP and total GFP_mRNA remain constant and in the yeast cells there is no active transport of GFP so parameters R_1, k_{1-4}, D_2 and D_3 can be set equal to 0. The resulting two equations can be solved using the initial conditions at the first post bleach frame for the normalised FRAP data giving the mono-exponential recovery curve in the nucleus,

$$[GFP]_{np} = 1 - e^{-2D_1 t} \qquad 22$$

This function was fitted to the normalised FRAP data using MATLAB. The rate, D_1, was found to be $0.1011s^{-1}$ (0.09808, 0.1041) for the WT cells and $0.1029s^{-1}$ (0.09778, 0.1081) for the ΔTether mutants with 95% confidence bounds.

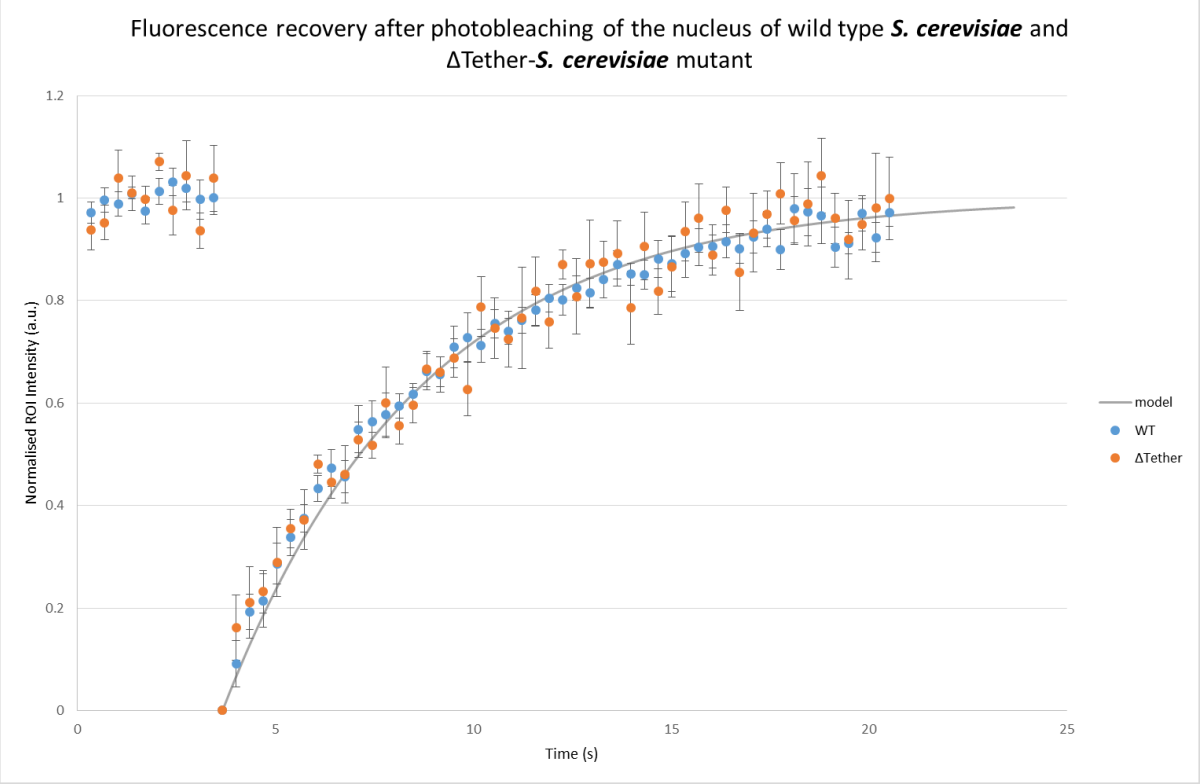

Figure 7: Data from FRAP of the nucleus in WT and ΔTether yeast. WT fit with mono-exponential shown has R² value of 0.967.

Conclusions

Modelling Nucleocytoplasmic Protein Shuttling In Fused Cells

To investigate the maintenance of nuclear independence, I have derived a model of nucleocytoplasmic shuttling of proteins in a pair of fused cells. This model has been used to fit data from a cell-cell fusion experiment where the accumulation of GFP-NLS, in the acceptor nucleus, was measured. The model demonstrates that a diffusion barrier, maintained between the fused cells, is not the only necessary condition to describe the rate of accumulation. Accordingly, the model incorporates multiple parameters important in regulating exchange between individual nuclei. The combined results of a parameter sensitivity analysis identify two factors which play a role in determining the half time of GFP-NLS accumulation in the acceptor nucleus. Firstly, the steady state ratio of nuclear to cytoplasmic concentrations and secondly, the resulting rates of diffusion into and out of the nucleus. These two factors, and the parameters that define them, are also strongly interacting. I therefore propose that an extensive parameter analysis is performed to measure the extent of these interactions. It is also necessary to fully quantify the sensitivity of each parameter and to characterise the uncertainty in the output of the model.

The parameters in the model need to be measured, by experiment, for a quantitative analysis of the particular system to be achieved. This is necessary as there are sets of biologically relevant parameters where a strong diffusion barrier could be a necessary and sufficient requirement to describe the observations. The parameterisation of the model could also be drastically simplified by experimental design for example by inhibition of new protein synthesis after fusion.

Experiments are currently being performed[‡] where as many as 10-20 cells can be fused with only one or two nuclei expressing GFP-NLS prior to fusion. In these experiments all acceptor nuclei appear to accumulate GFP-NLS at the same rate independent of distance to donor. Also, the accumulation appears to be sigmoidal rather than exponential as is predicted by the pair model. This sigmoidal behaviour is observed when mRNA concentrations are bellow there equilibrium concentration. I propose that a model of multiple cell fusions could be formed with three compartments, donor nuclei, acceptor nuclei and a common, continuous cytoplasm. At the point of cell fusion the initial conditions for each compartment would need to be determined by the single cell values modulated by the volume change. This would take the mRNA concentration away from its equilibrium value possibly resulting in the observed sigmoidal accumulation. This would be confounded if an additional, non-fluorescent, state corresponding to the unfolded GFP state was added[24].

The model I derived implies that nuclear independence in syncytia could be maintained by large nuclear to cytoplasmic concentration gradients. This could be confirmed or refuted however by experimentally modulating the diffusion rates in and out of the nucleus. Differing NLS and NES constructs could achieve this and results could be compared with previous fusion experiments. For example Howell, J. L. & Truant, R.[17] fused identical cells and used FRAP to show accumulation in the acceptor nucleus occurs much faster in the presence of NESs.

The Role of the Endoplasmic Reticulum in Nucleocytoplasmic Protein Shuttling

I have also measured the passive NE diffusion rate for GFP in WT and ΔTether ***S. cerevisiae*** using FRAP. The values found did not differ significantly implying the altered structure of the ER has not resulted in a change in the diffusion rate between the nucleoplasm and the cytoplasm.

I was unable, with the experimental set up available, to measure the rate of translational diffusion of GFP in the cytoplasm. This was due to the low time resolution it was possible to achieve at the required

[‡] Experiments being performed by B. Baum and S. Sarfati, data not shown.

spatial resolution on the SP5 confocal microscope. FRAP in the cytoplasm as a method for identifying compartmentalisation has, however, been achieved in bacteria.[36] More advanced methods such as FCS accompanied with appropriate analysis, for example lattice Boltzmann models, may also be employed to study diffusion in the cytoplasm.[37] Also, while anomalous diffusion is observed in bacteria without organelles and therefore attributed to molecular crowding and sieving[38]; my results do not indicate whether or not the ER and other organelles have a role to play in anomalous cytoplasmic diffusion and this should be investigated further.

Further to the work presented here, I propose that other methods for manipulating the architecture of the ER could be tested. For example changing expression of proteins such as reticulons which regulate ER curvature.[39] It is also possible to measure the diffusion rates of proteins in the ER lumin using FRAP[40] and ER localising constructs such as HDEL[41]. It may also be possible to determine the point of ER separation during budding and correlate this to the nuclear division and the point of cytokinesis measured by FRAP in the cytoplasm and ER of the bud.

Finally, I propose that these two studies are fully integrated. First, by investigating cytoplasmic diffusion of ER structure mutants in mammalian cells by FRAP. Second, by investigating the change in GFP-NLS accumulation in acceptor nuclei of cells with altered ER architecture.

Acknowledgements

I would like to thank Dr. C Stefan for the provision of yeast cells and plasmids and for assistance preparing samples and performing FRAP experiments. I would like to thank Dr. B. Baum for proving preliminary data for cell-cell fusion experiments. I would also like to thank Dr. C Stefan and Dr. B. Baum for offering and supervising this project and for their insight and discussion during the project.

References

1. Alberts, B., Johnson, A. & Lewis, J. *Molecular Biology of the Cell.* (Garland Science, 2002). at <http://www.ncbi.nlm.nih.gov/books/NBK26907/>

2. Baum, D. A. & Baum, B. An inside-out origin for the eukaryotic cell. *Nature* **In Press,** (2014).

3. Luby-Phelps, K., Taylor, D. L. & Lanni, F. Probing the structure of cytoplasm. *J. Cell Biol.* **102,** 2015–22 (1986).

4. Song, A.-H. *et al.* A selective filter for cytoplasmic transport at the axon initial segment. *Cell* **136,** 1148–60 (2009).

5. Seksek, O., Biwersi, J. & Verkman, a S. Translational diffusion of macromolecule-sized solutes in cytoplasm and nucleus. *J. Cell Biol.* **138,** 131–42 (1997).

6. Pavlath, G. K., Rich, K., Webster, S. G. & Blau, H. M. Localisation of muscle gene products in nuclear domains. *Nature* **337,** 570–573 (1989).

7. Rotundo, R. L. Nucleus-specific translation and assembly of acetylcholinesterase in multinucleated muscle cells. *J. Cell Biol.* **110,** 715–9 (1990).

8. Burden, S. J. Synapse-specific gene expression. *Trends Genet.* **9,** 12–6 (1993).

9. Sherlekar, A. & Rikhy, R. Drosophila embryo syncytial blastoderm cellular architecture and morphogen gradient dynamics: Is there a correlation? *Front. Biol. (Beijing).* **7,** 73–82 (2012).

10. Frescas, D., Mavrakis, M., Lorenz, H., Delotto, R. & Lippincott-Schwartz, J. The secretory membrane system in the Drosophila syncytial blastoderm embryo exists as functionally compartmentalized units around individual nuclei. *J. Cell Biol.* **173,** 219–30 (2006).

11. Gladfelter, A. S. Nuclear anarchy: asynchronous mitosis in multinucleated fungal hyphae. *Curr. Opin. Microbiol.* **9,** 547–52 (2006).

12. Gerstenberger, J. P., Occhipinti, P. & Gladfelter, A. S. Heterogeneity in mitochondrial morphology and membrane potential is independent of the nuclear division cycle in multinucleate fungal cells. *Eukaryot. Cell* **11,** 353–67 (2012).

13. Anderson, C. a *et al.* Nuclear repulsion enables division autonomy in a single cytoplasm. *Curr. Biol.* **23,** 1999–2010 (2013).

14. Friedman, J. R. & Voeltz, G. K. The ER in 3D: a multifunctional dynamic membrane network. *Trends Cell Biol.* **21,** 709–17 (2011).

15. Stefan, C. J., Manford, A. G. & Emr, S. D. ER-PM connections: sites of information transfer and inter-organelle communication. *Curr. Opin. Cell Biol.* **25,** 434–42 (2013).

16. Manford, A. G., Stefan, C. J., Yuan, H. L., Macgurn, J. a & Emr, S. D. ER-to-plasma membrane tethering proteins regulate cell signaling and ER morphology. *Dev. Cell* **23,** 1129–40 (2012).

17. Howell, J. L. & Truant, R. Live-Cell Nucleocytoplasmic Protein Shuttle Assay Utilizing Laser Confocal Microscopy and FRAP. *Biotechniques* **32,** (2002).

18. Furtado, A. & Henry, R. Measurement of green fluorescent protein concentration in single cells by image analysis. *Anal. Biochem.* **310,** 84–92 (2002).

19. Keminer, O. & Peters, R. Permeability of single nuclear pores. *Biophys. J.* **77,** 217–28 (1999).

20. Bizzarri, R., Cardarelli, F., Serresi, M. & Beltram, F. Fluorescence recovery after photobleaching reveals the biochemistry of nucleocytoplasmic exchange. *Anal. Bioanal. Chem.* **403,** 2339–51 (2012).

21. Renkin, E. M. Filtration, diffusion, and molecular sieving through porous cellulose membranes. *J. Gen. Physicology* **38,** 225–243 (1954).

22. Yang, E. *et al.* Decay rates of human mRNAs: correlation with functional characteristics and sequence attributes. *Genome Res.* **13,** 1863–72 (2003).

23. Ross, J. mRNA stability in mammalian cells. *Microbiol. Rev.* **59,** 423–50 (1995).

24. Subramanian, S. & Srienc, F. Quantitative analysis of transient gene expression in mammalian cells using the green fluorescent protein. *J. Biotechnol.* **49,** 137–51 (1996).

25. Press, W. H., Teukolsky, S. A., Vetterling, W. T. & Flannery, B. *Numerical Recipies in C.* (Cambridge Univeristy Press, 2007).

26. Heim, R., Cubitt, A. B. & Tsien, R. Y. Improved Green Fluorescence. *Nature* **373,** 663–664 (1995).

27. Reits, E. a & Neefjes, J. J. From fixed to FRAP: measuring protein mobility and activity in living cells. *Nat. Cell Biol.* **3,** E145–7 (2001).

28. Sprague, B. L. & McNally, J. G. FRAP analysis of binding: proper and fitting. *Trends Cell Biol.* **15,** 84–91 (2005).

29. Axelrod, D., Koppel, D. E., Schlessinger, J., Elson, E. & Webb, W. W. Mobility measurement by analysis of fluorescence photobleaching recovery kinetics. *Biophys. J.* **16,** 1055–69 (1976).

30. Poo, M. & Cone, R. Lateral diffusion of rhodopsin in the photoreceptor membrane. *Nature* **247,** 438–441 (1974).

31. Soumpasis, D. M. Theoretical Analysis of Fluorescence Photobleaching Recovery Experiments. *Biophys. J.* **41,** 95–97 (1983).

32. Ellenberg, J. *et al.* Nuclear membrane dynamics and reassembly in living cells: targeting of an inner nuclear membrane protein in interphase and mitosis. *J. Cell Biol.* **138,** 1193–206 (1997).

33. White, J. & Stelzer, E. Photobleaching GFP reveals protein dynamics inside live cells. *Trends Cell Biol.* **9,** 61–5 (1999).

34. Abràmoff, M. D., Hospitals, I., Magalhães, P. J. & Abràmoff, M. Image Processing with ImageJ. *Biophotonics Int.* **11,** 36–42 (2004).

35. Phair, R. D., Gorski, S. A. & Misteli, T. *Measurement of Dynamic Protein Binding to Chromatin In Vivo, Using Photobleaching Microscopy*. *Methods Enzymol.* **375,** 393–414 (Elsevier, 2003).

36. Schlimpert, S. *et al.* General protein diffusion barriers create compartments within bacterial cells. *Cell* **151,** 1270–82 (2012).

37. Kühn, T. *et al.* Protein diffusion in mammalian cell cytoplasm. *PLoS One* **6,** e22962 (2011).

38. Mika, J. T. & Poolman, B. Macromolecule diffusion and confinement in prokaryotic cells. *Curr. Opin. Biotechnol.* **22,** 117–26 (2011).

39. Yang, Y. S. & Strittmatter, S. M. The reticulons: a family of proteins with diverse functions. *Genome Biol.* **8,** 234 (2007).

40. Dayel, M. J., Hom, E. F. & Verkman, a S. Diffusion of green fluorescent protein in the aqueous-phase lumen of endoplasmic reticulum. *Biophys. J.* **76,** 2843–51 (1999).

41. Gomord, V. *et al.* The C-terminal HDEL sequence is sufficient for the retention of secretory proteins in the endoplasmic reticulum (ER) but promotes vacuolar targeting of proteins that escape the ER. *Plant J.* **11,** 313–325 (1997).